ADVANCED FUNCTIONAL MATERIALS
www.afm-journal.de

www.MaterialsViews.com

An Advanced Nitrogen-Doped Graphene/Cobalt-Embedded Porous Carbon Polyhedron Hybrid for Efficient Catalysis of Oxygen Reduction and Water Splitting

Yang Hou, Zhenhai Wen, Shumao Cui, Suqin Ci, Shun Mao, and Junhong Chen**

A novel hybrid electrocatalyst consisting of nitrogen-doped graphene/cobalt-embedded porous carbon polyhedron (N/Co-doped PCP//NRGO) is prepared through simple pyrolysis of graphene oxide-supported cobalt-based zeolitic imidazolate-frameworks. Remarkable features of the porous carbon structure, N/Co-doping effect, introduction of NRGO, and good contact between N/Co-doped PCP and NRGO result in a high catalytic efficiency. The hybrid shows excellent electrocatalytic activities and kinetics for oxygen reduction reaction in basic media, which compares favorably with those of the Pt/C catalyst, together with superior durability, a four-electron pathway, and excellent methanol tolerance. The hybrid also exhibits superior performance for hydrogen evolution reaction, offering a low onset overpotential of 58 mV and a stable current density of 10 mA cm^{-2} at 229 mV in acid media, as well as good catalytic performance for oxygen evolution reaction (a small overpotential of 1.66 V for 10 mA cm^{-2} current density). The dual-active-site mechanism originating from synergic effects between N/Co-doped PCP and NRGO is responsible for the excellent performance of the hybrid. This development offers an attractive catalyst material for large-scale fuel cells and water splitting technologies.

1. Introduction

The impending global energy crisis has prompted intense research on energy conversion and storage systems.[1] Electrocatalytic oxygen reduction reaction (ORR), hydrogen evolution reaction (HER), and oxygen evolution reaction (OER) play key roles in various energy technologies, including fuel cells[2] and water splitting.[3] The development of highly efficient electrocatalysts for ORR, HER, and OER is the key for these applications. To date, most efficient catalysts for ORR, HER, and OER contain precious metals;[4] however, the high cost and scarcity of these precious metals severely limit their applications.[5] Thus, it is important to discover efficient and low-cost electrocatalysts to replace precious metal-based catalysts. Nitrogen/transition metal (Cobalt-based)-doped carbon materials have been recognized as one of the most promising candidates owing to their low cost and high catalytic activity.[6] The electrocatalytic performance of these modified-carbon materials is strongly governed by their structures and morphologies.[7] Despite the tremendous progress in the synthesis of carbon materials, such as graphene,[8] carbon nanotubes,[9] and porous carbons,[10] it still remains a challenge to design and synthesize a porous carbon polyhedron (PCP) catalyst with the merits of high activity, large surface area, and excellent stability. Moreover, previously reported carbon-based electrocatalysts exhibit excellent catalytic activity for either ORR,[11] HER,[12] or OER,[13] but high triple activity for ORR, HER, and OER using carbon-based electrocatalyvsts have rarely been reported.[14] Therefore, the development of multifunctional nitrogen/cobalt-doped PCP (N/Co-doped PCP) electrocatalysts is highly desirable.

Recently, nitrogen-doped reduced graphene oxide (NRGO) has gained noticeable popularity as a candidate for electrochemical applications because of its excellent electrical properties and abundant active sites.[15] Combining an N/Co-doped PCP catalyst with NRGO sheets to form a hybrid is an effective strategy to integrate their respective merits and to enhance the overall catalytic activity. To the best of our knowledge, there has been no report on controllable synthesis of N/Co-doped PCP catalyst supported on NRGO sheets as ORR, HER, and OER catalysts simultaneously.

Herein, we demonstrate a novel nitrogen-doped graphene/cobalt-embedded porous carbon polyhedron (N/Co-doped PCP//NRGO) hybrid electrocatalyst obtained through a simple pyrolysis of graphene oxide (GO) and a zeolitic imidazolate-framework (ZIF), ZIF-67, followed by partially etching away metallic cobalt. ZIF-67 was chosen as one of the most ideal candidates owing to its advantages of abundant Co–N moieties and unique dodecahedral morphology,[16] which may be a suitable precursor to yield a N/Co-doped PCP. Significantly, this is the first report on the N/Co-doped PCP//NRGO hybrid with triple activity for ORR, HER, and OER catalysis. The electrocatalytic characterization shows that the as-synthesized hybrid possesses excellent electrocatalytic activities for the ORR, HER, and OER with good stability. The enhanced performance of the hybrid catalyst is likely correlated with dual-active-site mechanisms originating from the synergic effects between N/Co-doped PCP and NRGO sheets.

Dr. Y. Hou, Dr. Z. H. Wen, Dr. S. M. Cui, Dr. S. Q. Ci, Dr. S. Mao, Prof. J. H. Chen
Department of Mechanical Engineering
University of Wisconsin-Milwaukee
3200 North Cramer Street, Milwaukee
WI 53211, USA
E-mail: wenzhenhai@yahoo.com; jhchen@uwm.edu

DOI: 10.1002/adfm.201403657

2. Results and Discussion

The fabrication process for the N/Co-doped PCP//NRGO hybrid is demonstrated in **Figure 1**a. Highly uniform ZIF-67 polyhedrons were first synthesized by a simple solution-phase approach.[17] The obtained ZIF-67 samples were further dispersed in the GO solution (ZIF-67/GO) under stirring. The resulting ZIF-67/GO powders after drying at 80 °C were then thermally treated under flowing argon at 900 °C, and finally etched in acid to form a N/Co-doped PCP//NRGO hybrid. During this process, the continuous decomposition of ZIF-67 polyhedrons was accompanied by the release of nitrogen-containing gases,[18] which resulted in the formation of a porous carbon structure incorporating cobalt nanoparticles, as shown by the thermogravimetric analysis (TGA) results (Figure S1, Supporting Information). Simultaneously, the nitrogen-containing species contributed to the reduction of GO and nitrogen doping in both GO and porous carbon, finally evolving into the N/Co-doped PCP//NRGO hybrid (Figure S2, Supporting Information).

Field emission scanning electron microscopy (FESEM) images (Figure 1b,c) show that the ZIF-67 possesses a regular rhombic dodecahedral morphology composed of twelve equivalent rhombus faces, twenty edges, and sixteen vertices, with an average edge length of 500 nm. Compared with ZIF-67, N/Co-doped PCP retained the rhombic dodecahedral structure well, although its surface became rough and the corresponding size decreased a little (≈400 nm) due to the decomposition and shrinkage during the annealing process (Figure 1d). The porous structures are clearly observed from irregularly shaped pores randomly located on the surface of the N/Co-doped PCP (indicated by arrows, Figure 1e), which are favorable for electrolyte filling and enable rapid electron transport. However, we did not observe the presence of metallic cobalt nanoparticles in the N/Co-doped PCP, possibly due to the nanoparticles inside the PCP with a low concentration. In fact, the presence of a small amount of metallic cobalt has been proven to be beneficial for the improvement of electrocatalytic activities toward ORR and HER.[19] FESEM images of N/Co-doped PCP//NRGO reveal that the hybrid consists of many N/Co-doped PCP and

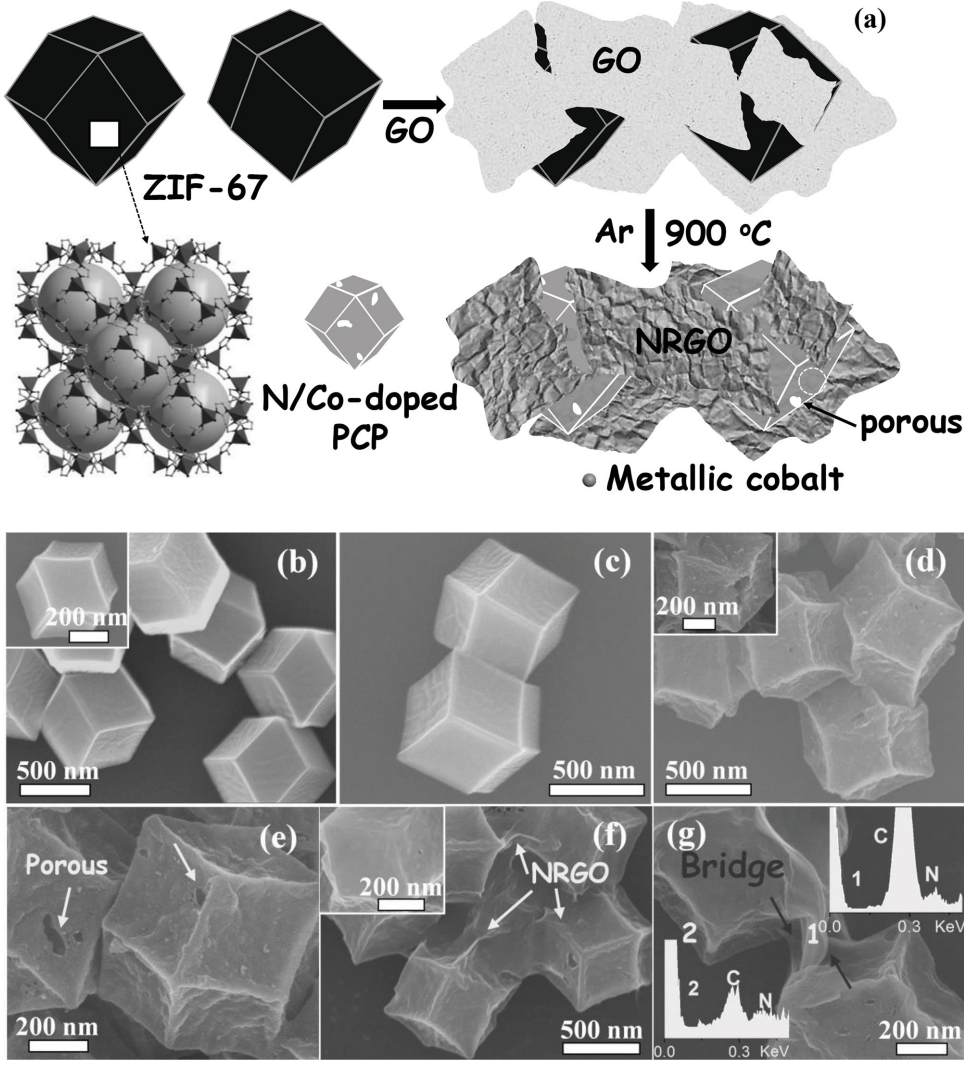

Figure 1. a) Schematic illustration for the synthesis process of N/Co-doped PCP//NRGO. FESEM images of b–c) ZIF-67, d–e) N/Co-doped PCP, and f–g) N/Co-doped PCP//NRGO. Inset: the corresponding EDX spectra.

NRGO sheets (Figure 1f). Energy-dispersive X-ray spectroscopy analysis confirmed the co-existence of N elements on the PCP and NRGO sheets in the hybrid (Figure 1g). Crumpled NRGO sheets wrapped around the surface of the N/Co-doped PCP and also bridged nearby N/Co-doped PCP together, indicating that a close interfacial contact between N/Co-doped PCP and NRGO sheets was formed. The content of NRGO sheets in the hybrid was calculated as ≈8.3 wt% from TGA results (Figure S3, Supporting Information). Elemental mapping images of the N/Co-doped PCP//NRGO disclose the well-defined spatial distribution of all elements C, N, and Co in the hybrid (Figure S4, Supporting Information).

The morphology and structure of the N/Co-doped PCP// NRGO was further investigated by transmission electron microscopy (TEM). **Figure 2**a shows a typical TEM image of a single ZIF-67 rhombic dodecahedron with a smooth surface, which is in good agreement with the FESEM observation. After thermal and acid treatments, the ZIF-67 rhombic dodecahedron was converted to N/Co-doped PCP with a side length of 300–400 nm. The PCP was composed of numerous cobalt nanoparticles (about 12 nm in diameter) and continuous carbon networks (Figure 2b,c). The high-resolution TEM (HRTEM) image clearly shows that the cobalt nanoparticles were enclosed by carbon layers, which is attributable to the catalytic effect of Co ions on graphitization (Figure 2d).[20] The measured lattice spacing of 0.34 nm is slightly larger than that for graphite (0.335 nm), suggesting that the stacking of the graphitic layers has experienced some distortion (turbostratic structure). The crystalline cobalt and carbon shells are further proved from the selected area electron diffraction (SAED) pattern (Inset of Figure 2b) from scattered dots (cobalt) and diffraction rings (carbon).[21] Further observation revealed the presence of many mesopores in the carbon networks (Figure 2e and Figure S5, Supporting Information), mainly due to the graphitization of amorphous carbon catalyzed by cobalt metal, the removal of metallic cobalt after leaching (Figure S6, Supporting Information), and the release of carbon/nitrogen mixed gases;[22] thus, better exposure and enhanced utilization of electroactive sites (e.g., Co and N species) on the large active surface of N/Co-doped PCP greatly contribute to its high catalytic activity. Notably, some of the carbon networks were disordered (indicated by circles, Figure 2e), which may be attributed to the doping of hetero-atoms N that can lead to the stacking disorder and a turbostratic structure of the graphitic planes.[23] As for N/Co-doped PCP//NRGO, the NRGO sheets with crinkled textures are clearly observed on the surface of the N/Co-doped PCP, indicating that the N/Co-doped PCPs are surrounded and wrapped by NRGO sheets (Figure 2f). The HRTEM image clearly displays the structural distribution among cobalt nanoparticles, carbon networks, and NRGO sheets (Figure 2g). In the structure, both carbon networks and NRGO sheets can serve not only as conduction paths for shuttling electrons but also as active sites for the electrocatalytic process (see below). The well-resolved lattice fringes with an interplane distance of 0.20 nm come from the (111) plane of metallic cobalt.[18]

The XRD pattern of the N/Co-doped PCP shows the disappearance of the ZIF-67 nanostructure with the appearance of two prominent diffraction peaks at 26.0° and 43.0°, corresponding with the (002) and (110) reflections of turbostratic carbon, respectively (**Figure 3**a). The remaining peaks at 44.2° and 51.5° can be indexed to crystalline facets of Co (111) and Co (200) (JCPDS No. 15–0806), suggesting the successful reduction of the Co ions to a metallic state after carbonization. The calculated particle size of the cobalt using the Scherrer equation was about 10 nm,[24] which is in good agreement with the observation from the TEM images. With the introduction of NRGO, the peak at 26.0° becomes stronger and broader, which may be due to the overlap from two diffraction peaks related to the (002) planes of N/Co-doped PCP and NRGO. The Raman spectrum of the N/Co-doped PCP shows characteristic D and G bands at 1332 and 1584 cm^{-1}, which are associated with the disordered carbon atoms and sp2 hybridized graphitic carbon atoms, respectively (Figure 3b).[25] The intensity ratio of I_D/I_G is about 1.01. The G band of N/Co-doped PCP//NRGO downshifts to 1577 cm^{-1}, and the I_D/I_G value of the hybrid increases to 1.12, which implies that there are more defects in the hybrid caused by the introduction of NRGO sheets.[26] The increased defects may result from the disordered RGO edges by elimination of pendant functional groups in GO sheets, and the incorporation of heterogeneous N atoms into the RGO layers.[27] In addition, the G band of the RGO red-shifts to 1590 cm^{-1} and the ratio of I_D/I_G decreases to 1.07 compared with the hybrid, which may be due not only to the existence of PCP in the N/Co-doped PCP//NRGO, but also to the generation of more defective structures from the partial incorporation of N-atoms during the decomposition of ZIF-67.[28] Such phenomenon is commonly observed in N-doped graphene materials because the insertion of nitrogen atoms can cause distortion of the sp2 carbon lattice of graphene.[29] Therefore, the results provide evidence for the incorporation of N atoms into the RGO.

To probe the chemical composition and the effect of doping in the N/Co-doped PCP//NRGO, X-ray photoelectron spectroscopic (XPS) measurements were carried out and showed the presence of C, N, Co, and O (Figure S7, Supporting Information). The high-resolution N 1s spectrum can be deconvoluted into five peaks, corresponding with pyridinic-N (397.5 eV), Co-N (399.1 eV), pyrrolic-N (400.4 eV), graphitic-N (402.2 eV), and oxidized-N (404.6 eV), respectively, all of which play an important role in the ORR, HER, and OER processes except the oxidized-N specie (Figure 3c and Figure S8, Supporting Information).[13,18,19b] The atomic percentage of doped nitrogen was about 3.5 at% (Table S1, Supporting Information). Deconvolution of the complex Co 2p spectrum suggests the presence of two chemically distinct species: metallic Co (778.0 eV) and Co^{2+} species (781.7 eV and 788.0 eV).[30] The latter is probably derived from surface oxidation of metallic Co in air.[18] Notably, the surface content of cobalt in the hybrid is only about 0.5 at% after etching (Table S1, Supporting Information). Additionally, the intensity of C 1s peaks for carbon atoms bonded to oxygen decreased rapidly in the hybrid, indicating that most of the oxygen groups were removed (Figure S9, Supporting Information).[31] Infrared spectroscopy (IR) measurements showed that after thermal treatment (Figure S10, Supporting Information), almost all of the oxygen functional groups, such as C=O (1728 cm^{-1}) and C-OH (1235 cm^{-1}) bonds, vanished in the hybrid, indicating an effective reduction of GO.[32] The new band observed in the 1616–1342 cm^{-1} region was related to the vibrations of C=C and C=N,[33] which further confirms the

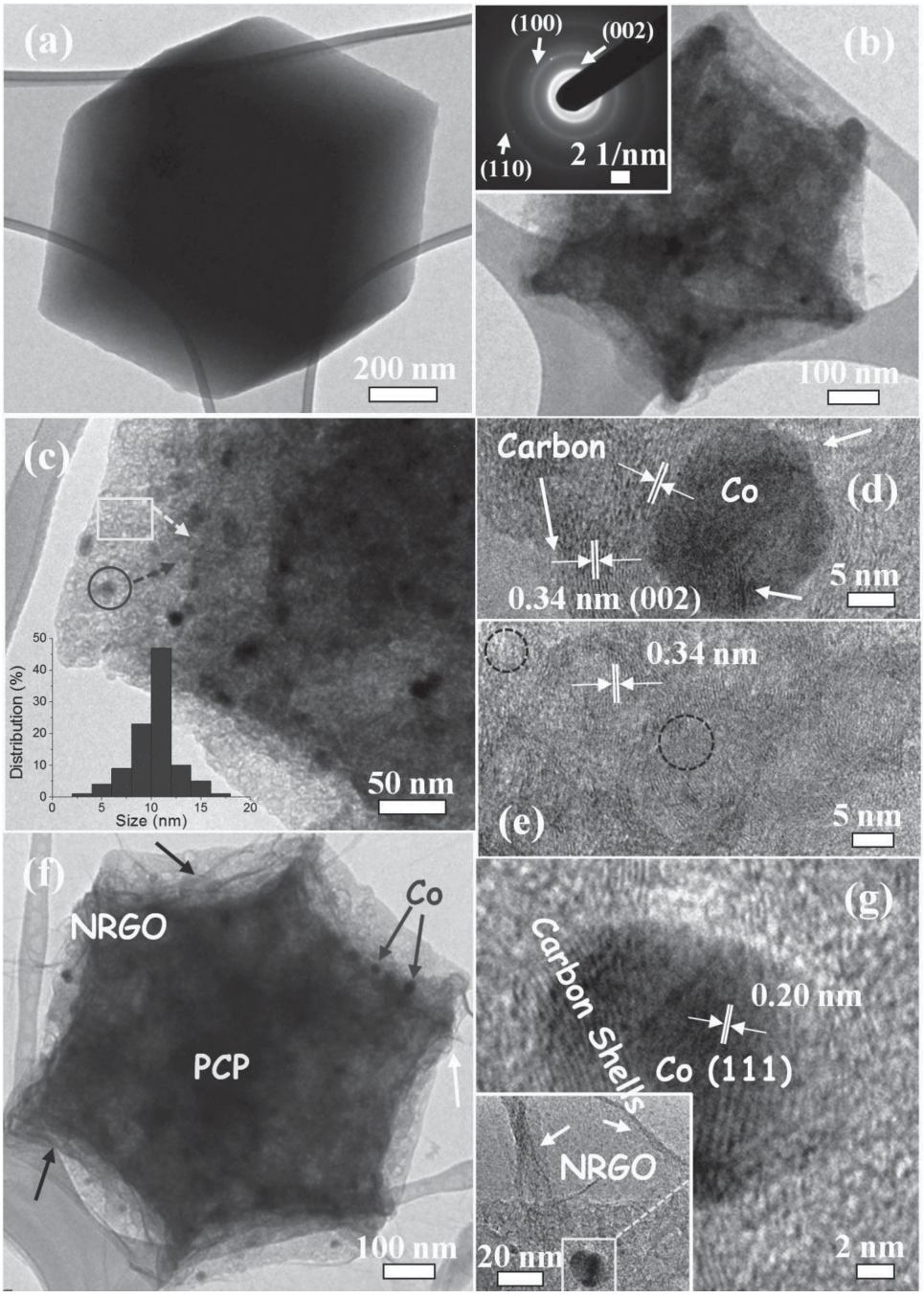

Figure 2. TEM images, SAED pattern, and HRTEM images of a) ZIF-67, b–e) N/Co-doped PCP, and f–g) N/Co-doped PCP//NRGO. Inset in (c): size histograms of cobalt nanoparticles. (d) and (e) show HRTEM images of N/Co-doped PCP//NRGO from the areas labeled by the circle and rectangular frames in (c), respectively. The arrows in (d), (f), and (g) are carbon shells (red) and NRGO sheets (blue and white).

successful doping of nitrogen. The Brunauer–Emmett–Teller (BET) surface area of the N/Co-doped PCP//NRGO was 375 $m^2 g^{-1}$ (Figure 3d and Table S2, Supporting Information), which is much higher than those of the N/Co-doped PCP before etching (237 $m^2 g^{-1}$), N/Co-doped PCP (266 $m^2 g^{-1}$), and physical mixture (304 $m^2 g^{-1}$), respectively. The larger surface area is anticipated to provide more active sites, likely leading to a higher electrocatalytic activity.

To evaluate the electrocatalytic activity of N/Co-doped PCP//NRGO for ORR, rotating disk electrode experiments were conducted in 0.1 M KOH solution (**Figure 4**a). All potentials used were referenced to a reversible hydrogen electrode (RHE). N/Co-doped PCP//NRGO exhibited a pronounced electrocatalytic ORR activity associated with a more positive ORR onset potential (0.97 V) and a higher steady-state cathodic current density (7.53 mA cm^{-2} at 0.4 V) than for N/Co-doped PCP (0.93 V,

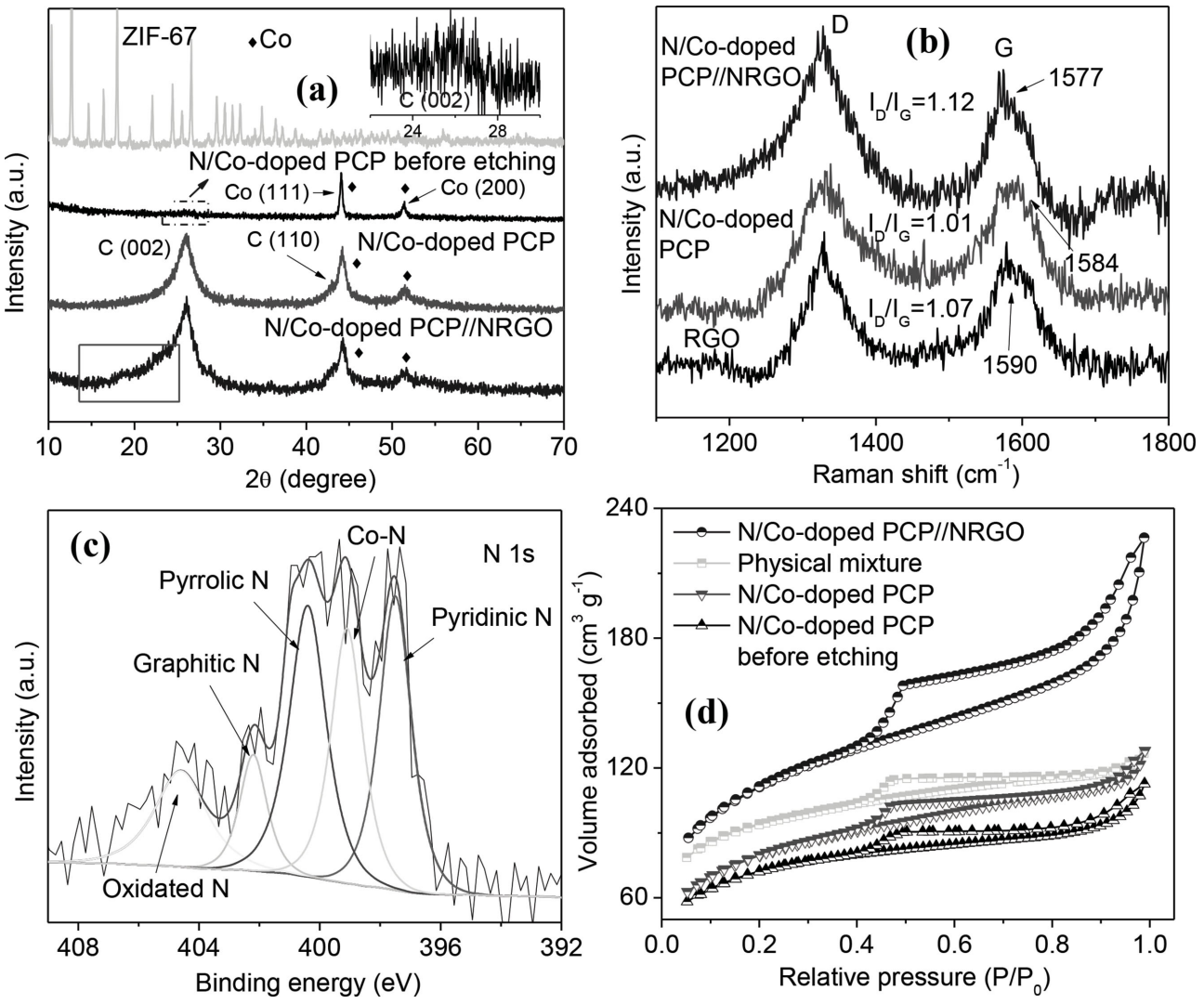

Figure 3. a) XRD patterns, b) Raman spectra, c) high-resolution N 1s XPS spectrum, and d) Nitrogen adsorption-desorption isotherm curves of N/Co-doped PCP before etching, N/Co-doped PCP, and N/Co-doped PCP//NRGO. Data for ZIF-67, RGO, and physical mixture are also shown.

3.76 mA cm^{-2} at 0.4 V) (Figure 4b and Figure S11, Supporting Information). However, the NRGO sheets alone showed a poor ORR catalytic activity (0.87 V, 2.07 mA cm^{-2} at 0.4 V). The results confirmed that the NRGO introduction significantly enhanced the ORR catalytic activity of N/Co-doped PCP, which in turn confirmed that the N/Co-doped PCP can be the active site to boost ORR. In the hybrid, NRGO sheets not only serve as a conduction path for shuttling electrons but also act as an active site for ORR (Figure S2, Supporting Information). Based on impedance spectroscopy measurements (Figure S12, Supporting Information), the N/Co-doped PCP//NRGO exhibited a smaller semicircle than did the N/Co-doped PCP in the Nyquist plots, suggesting a smaller charge transfer resistance in the hybrid during ORR, likely due to a lower charge transfer impedance for the hybrid than the N/Co-doped PCP.

To confirm the synergic effect between N/Co-doped PCP and NRGO, we compared the ORR activities of the hybrid with an ex situ synthesized hybrid (N/Co-doped PCP-RGO). The onset potential and steady-state cathodic current density for the N/Co-doped PCP-RGO were 0.94 V and 5.26 mA cm^{-2} at 0.4 V, which are superior to N/Co-doped PCP but are much lower than those for N/Co-doped PCP//NRGO. Assuming that the electrical conductivity of N/Co-doped PCP with RGO or NRGO is comparable (due to the small amount of N-doping), the difference was caused by the increase of structure defects in the hybrid originating from the N-doping of RGO sheets. Those defects (such as CN_x structures) can serve as additional active sites to contribute to the improvement of catalytic activity,[34] which is in accordance with theoretical studies that the substitution of carbon by *N* atoms could result in the formation of disordered carbon nanostructures, and incorporation of N-donated electrons to carbon,[35] thus facilitating the ORR. Notably, there is increasing evidence suggesting that N doping into carbon is critical to enhancing catalytic activity for the ORR, HER, and OER.[36] Thus, it is reasonable to deduce that there are two types of active sites in the hybrid: N/Co-doped PCP and NRGO sheets. Proper combination of the two, as seen in the hybrid, has a significant synergic effect on enhancing the catalytic activity. The

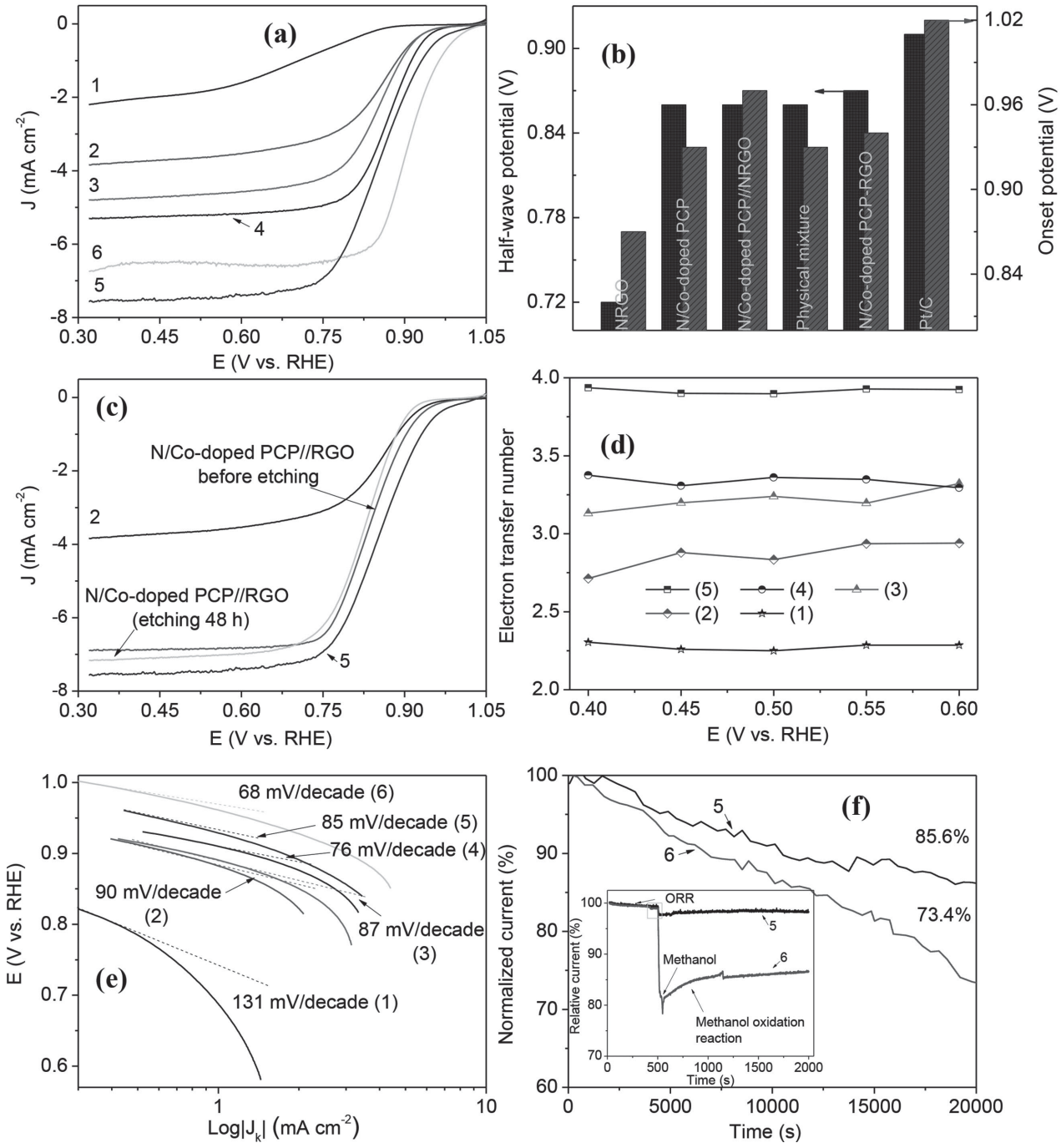

Figure 4. a) LSV curves of NRGO (1), N/Co-doped PCP (2), physical mixture (3), N/Co-doped PCP-RGO (4), N/Co-doped PCP//NRGO (5), and Pt/C (6) at a rotation rate of 1600 rpm in O_2-saturated 0.1 M KOH solution. b) The coresponding half-wave potentials and onset potentials of (1), (2), (3), (4), (5), and (6). c) LSV curves of (2), N/Co-doped PCP//NRGO before etching, N/Co-doped PCP//NRGO (etching 48 h), and (5) at a rotation rate of 1600 rpm in O_2-saturated 0.1 M KOH solution. d) Electron transfer numbers of (1), (2), (3), (4), and (5) as a function of the electrode potential; e) Tafel plots derived from Figure 4a. f) Current–time chronoamperometric responses of (5) and (6) at 0.9 V in O_2-saturated 0.1 M KOH solution (1600 rpm). Inset: chronoamperometric responses of (5) and (6) at 0.9 V in O_2-saturated 0.1 M KOH solution (1600 rpm) followed by 3 M methanol.

physical mixture of N/Co-doped PCP and NRGO sheets with an onset potential of 0.93 V and a steady-state cathodic current density of 4.75 mA cm^{-2} at 0.4 V shows improved catalytic activity compared with each individual component alone, but this mixture is still inferior to the hybrid in activity, indicating that good contact between N/Co-doped PCP and NRGO is crucial for the interfacial charge transfer. Direct pyrolysis of ZIF-67/GO hybrid precursors can afford strong chemical and electrical coupling between N/Co-doped PCP and NRGO sheets, allowing for rapid electron transfer from active materials to current collectors.[37]

In order to clarify the role of metallic cobalt in the ORR, control experiments were performed (Figure 4c). Remarkably, the N/Co-doped PCP//NRGO before etching (higher cobalt loading) showed a more negative ORR onset potential (0.93 V) with a lower steady-state cathodic current density (6.88 mA cm^{-2} at 0.4 V) than the N/Co-doped PCP//NRGO. However, the N/Co-doped PCP//NRGO after 48 h etching with a lower amount of cobalt loading (Table S1, Supporting Information), almost did not show improvement in catalytic activity compared with the N/Co-doped PCP//NRGO in terms of the steady-state cathodic current density (7.11 mA cm^{-2} at 0.4 V) and the onset potential (0.92 V), although it possessed a larger surface area (403 m^2 g^{-1}) and a higher nitrogen content of 3.9 at% than the N/Co-doped PCP//NRGO (Figure S13, Supporting Information). The results suggest that a significant enhancement of ORR catalytic activity was achieved by the introduction of appropriate cobalt content. The cobalt species can be stripped by nitrogen atoms to form Co–N sites in the carbon matrix, which are considered to be other active sites for ORR.[6] Density functional calculations revealed the enclosed Co-coordinated nitrogen complex reduced the oxygen adsorption energy of carbon surfaces and made the reduction of oxygen more easily.[38] Besides, more and more evidence has been presented showing that the geometric confinement of cobalt nanoparticles within the nitrogen-doped carbon structures contributes to highly active Co–N sites.[18,39] Especially, X-ray absorption fine-structure analyses have been reported to confirm the Co–N binding configurations.[40] The presence of the Co–N species in the hybrid may be supported by the formation of Co–N bonding in IR spectra (Figures S10 and S14, Supporting Information). Although the exact nature of the active sites in Co–N–C catalysts is still being debated, we believe more direct evidences for the active sites of N/Co-doped PCP may be obtained by rational design of micro/nano level electrochemical experiments and introducing advanced characterization methods (such as scanning electrochemical microscopy[41] and scanning tunneling microscopy,[42] etc.). These are beyond the scope of this paper and are thus not studied here. Impressively, the onset potential for N/Co-doped PCP//NRGO is close to that of the commercial Pt/C catalyst (1.02 V, 10 wt% Pt on Vulcan XC-72), but the steady-state cathodic current density of the former is higher than that of the Pt/C at 0.4 V, suggesting a pronounced electrocatalytic activity of N/Co-doped PCP//NRGO. Moreover, the high ORR activity of the N/Co-doped PCP//NRGO hybrid was comparable to, or even higher than, the other doped nanocarbons (Table S3, Supporting Information).

The electron transfer number (n) of N/Co-doped PCP//NRGO was calculated as 3.90–3.94 at 0.4–0.6 V (Figure 4d) according to the Koutecky–Levich equation (Equations (1)–(3), Supporting Information),[43] suggesting a four-electron transfer process; this result was reconfirmed by tests with a rotating ring–disk electrode (Figure S15, Supporting Information). The mechanism of the four-electron transfer for ORR has been suggested to proceed through simultaneous two-oxygen atom side and/or bridge adsorption for oxygen dissociation.[44] In contrast, N/Co-doped PCP-RGO, physical mixture, N/Co-doped PCP, and NRGO exhibited much lower n values of 3.31–3.37, 3.13–3.32, 2.71–2.94, and 2.25–2.30 at 0.4–0.6 V, respectively. In addition, the kinetic current densities (J_k) were maximized for N/Co-doped PCP//NRGO and decreased in the order of Pt/C > N/Co-doped PCP-RGO > physical mixture > N/Co-doped PCP > NRGO, with J_k values of 11.66, 8.28, 5.04, 4.28, 2.25, and 0.51 mA cm^{-2}, respectively, at 0.7 V (Figure S16 Supporting Information). The mass activity of N/Co-doped PCP//NRGO is 16.33 mA mg^{-1}_{cat} at 0.7 V, which is about 5.18 and 22.68 times greater than those of the N/Co-doped PCP (3.15 mA mg^{-1}_{cat}) and the NRGO (0.72 mA mg^{-1}_{cat}), respectively (Figure S17, Supporting Information). The excellent ORR activity of the N/Co-doped PCP//NRGO hybrid was further confirmed by the much smaller Tafel slope (Figure 4e, 85 mV/decade) at low overpotentials than that measured for N/Co-doped PCP (90 mV/decade) and NRGO (131 mV/decade), which is comparable to that of the Pt/C (68 mV/decade) The smaller Tafel slope corresponds with a more favorable ORR kinetics over the hybrid, reconfirming a synergic contribution of N/Co-doped PCP and NRGO sheets toward ORR.

Besides a high activity, the N/Co-doped PCP//NRGO hybrid also exhibited excellent stability as measured by chronoamperometric measurements (Figure 4f). After 20 000 s of reaction at 0.9 V, 85.6% of the current density of N/Co-doped PCP//NRGO toward ORR can be maintained, which is higher than that of the Pt/C catalyst (73.4%). More importantly, the N/Co-doped PCP//NRGO also exhibited better methanol tolerance than commercial Pt/C catalysts, which is very important for practical applications. A sharp decrease in the current density upon the addition of 3 M methanol was observed for the Pt/C catalyst (Inset of Figure 4f). In contrast, the N/Co-doped PCP//NRGO hybrid catalyst was only slightly affected by methanol (98% retention).

We also investigated the electrocatalytic activity of the N/Co-doped PCP//NRGO hybrid for HER in Ar-saturated 0.5 M H_2SO_4 solution. The polarization curve recorded with N/Co-doped PCP showed an onset overpotential of 129 mV for the HER (**Figure 5**a), beyond which the cathodic current rose rapidly under more negative potentials. Benefiting from the introduction of NRGO sheets, the N/Co-doped PCP//NRGO exhibited a much smaller onset overpotential value of 58 mV, which was only marginally lower than that of commercial Pt/C (negligible overpotential) under the same conditions, suggesting the superior HER activity. In sharp contrast, NRGO alone exhibited a little HER activity (onset overpotential of 340 mV). Moreover, a large cathodic current density of 96.7 mA cm^{-2} was obtained for the hybrid at –0.4 V, which was much higher than those observed for NRGO (2.1 mA cm^{-2}) and N/Co-doped PCP (16.9 mA cm^{-2}). Notably, for driving a current density of 10 mA cm^{-2}, the hybrid only required an overpotential of 229 mV, which made N/Co-doped PCP//NRGO among the most active nonprecious HER electrocatalysts in acidic solution (Table S4, Supporting Information), together with cobalt-embedded nitrogen-rich carbon nanotubes,[19b] Fe/N-rich tungsten carbonitride,[45] $Co_{0.6}Mo_{1.4}N_2$,[46] and FeCo-alloy into nitrogen-doped carbon nanotubes,[47] N,P-graphene,[48] and B-doped graphene.[49] These catalyst systems exhibited overpotentials that range from 200 to 450 mV at cathodic current densities of 10 mA cm^{-2}. The dramatic enhancement in catalytic activity was even more apparent upon comparison of the slopes of Tafel plots (Figure 5b) for the N/Co-doped PCP//NRGO (126 mV/decade) and N/Co-doped PCP (170 mV/decade). The earlier

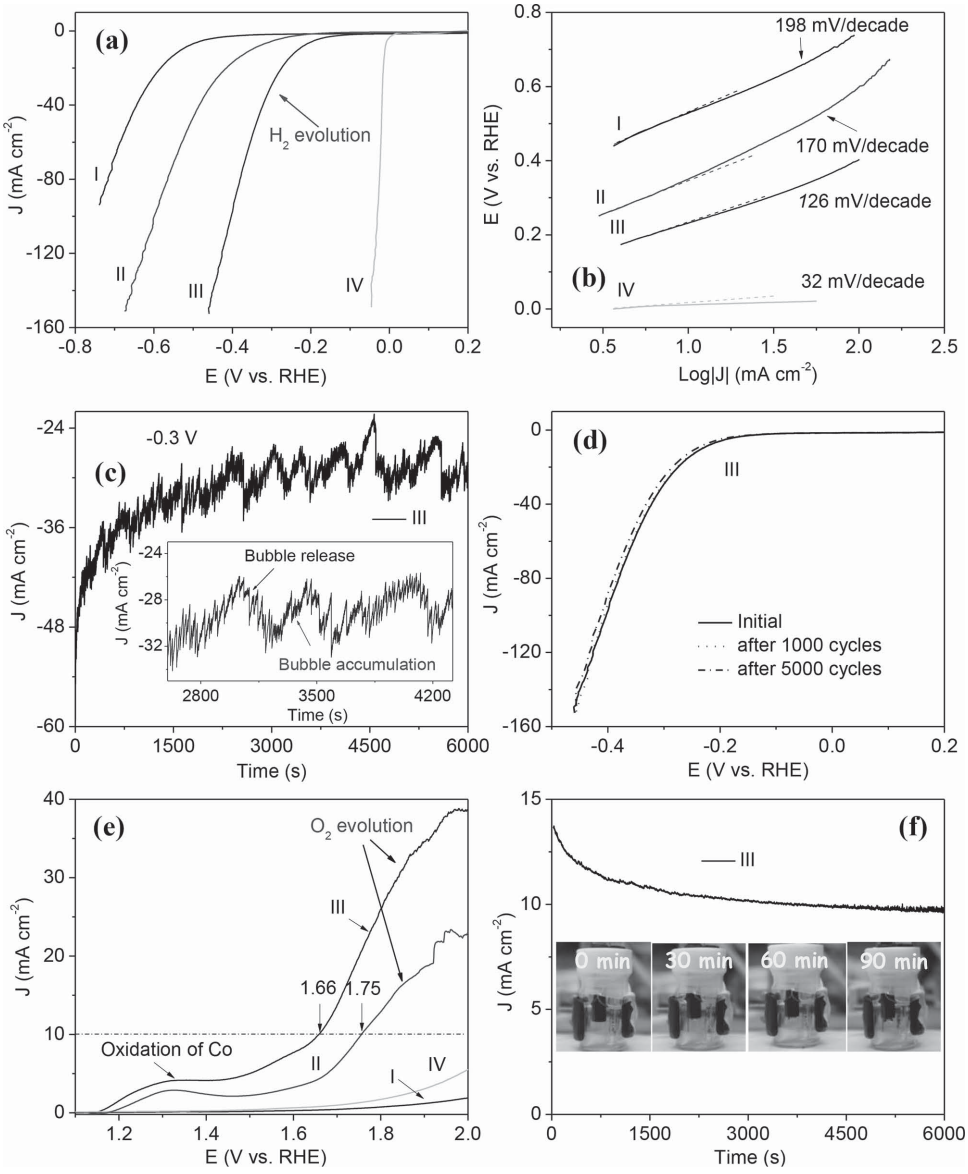

Figure 5. a) Polarization curves and b) corresponding Tafel plots of the NRGO (I), N/Co-doped PCP (II), N/Co-doped PCP//NRGO (III), and Pt/C (IV) at 5 mV s^{-1} in 0.5 M H_2SO_4 solution. The IR drop was corrected. c) Time dependence of cathodic current density during electrolysis at –0.3 V. d) Durability test for the (III). e) LSV curves of I, II, III, and IV at 5 mV s^{-1} in 0.1 M KOH solution. f) Chronoamperometric response for III at 1.7 V.

onset of catalytic activity and a smaller Tafel slope can be attributed to the synergic effect between N/Co-doped PCP and NRGO. Although the hetero-atom-doped carbon materials as active sites for HER has been recognized by numerous experimental and theoretical studies,[48,49] the exact nature of the active sites in N/Co-doped PCP remains unknown. Based on above result, coupled with the recent theoretical calculations on metal/nitrogen-doped carbon nanomaterials,[47] we think that introduction of metal and nitrogen dopants can synergistically optimize the electronic structure of the carbon and the adsorption energy of H atoms on carbon, thus promoting the electron transfer from metal/N-dopants to the carbon where HER occurs. Importantly, the stable current density over 6000 s of continuous operation suggests that the N/Co-doped PCP//NRGO hybrid possesses good stability for HER in acid solution. The typical serrate shape (Inset of Figure 5c) can be attributed to the alternating processes of H_2 bubble accumulation and release.[50] Only a slight decrease in the current was observed after 5000 cycles (Figure 5d), suggesting the high durability of N/Co-doped PCP//NRGO.

Excitingly, besides high ORR and HER activities, the N/Co-doped PCP//NRGO hybrid also exhibied a good OER catalytic performance (Figure 5e). The higher OER current density and an earlier onset of catalytic current was observed for N/Co-doped PCP//NRGO compared with N/Co-doped PCP, NRGO, and Pt/C, indicating that the hybrid is a highly active OER catalyst. An anodic peak of the hybrid is seen around 1.33 V preceding the oxygen evolution, which can be attributed to the fact that metallic cobalt nanoparticles in the hybrid were partly oxidized into cobalt oxide to form the cobalt oxide/cobalt

complex species.[51] The metallic cobalt nanoparticles, rather than cobalt oxide, were selected mainly due to their high conductivity which can improve charge transport of electrodes. The current density of 10 mA cm^{-2} can be achieved at a small overpotential of 1.66 V for the hybrid, lower than those of N/Co-doped PCP (1.75 V) and NRGO (>2 V), implying the superior OER activity of the hybrid originating from the synergic effect between N/Co-doped PCP and NRGO sheets. Similarly to the ORR, the introduction of metal/N dopants was proposed to render the adjacent carbon atoms positively charged. The positive carbon atoms can facilitate adsorption of OH ions, promote the electron transfer between the catalyst surface and reaction intermediates, resulting in the OER.[29,52] Significantly, the overpotential of the hybrid was comparable to those of other reported OER catalysts, including N-doped graphene/single-walled carbon nanotube hybrid (1.63 V vs RHE),[53] N-doped graphite (1.61 V vs RHE),[11] crumpled graphene/CoO (1.65 V vs RHE),[51] $Mn_3O_4/CoSe_2$ hybrid (1.68 V vs RHE),[54] $CaMn_4O_x$ (1.77 V vs RHE),[55] Mn_xO_y nanoparticles embedded nitrogen-doped carbon (1.68 V vs RHE),[52b] and rutile IrO_2 (1.68 vs RHE).[56] As for Pt/C, the overpotential acquired for the current density of 10 mA cm^{-2} would be much more positive, as deduced from the corresponding current trend. Besides, the enhanced kinetics (Figure S18, Supporting Information) of N/Co-doped PCP//NRGO toward OER is proved by its smaller Tafel slope of 292 mV/decade than that of N/Co-doped PCP (393 mV/decade). The high stability of N/Co-doped PCP//NRGO was observed in the chronoamperometric test, which showed a small current density change after 6000 s (Figure 5f). Moreover, the large amounts of oxygen bubbles evolved during the OER reaction can be seen clearly in the inset of Figure 5f.

The remarkable features of high activity, favorable kinetics, and strong durability suggest that the N/Co-doped PCP//NRGO is a promising electrocatalyst for electrochemical reactions of ORR, HER, and OER. Importantly, the hybrid can work well in both acidic (HER) and basic media (ORR and OER), which are rare properties for electrocatalysts.[57] Considering that the cost of raw materials for preparing N/Co-doped PCP//NRGO is also cheaper than that of the commercial Pt/C catalyst, based on the evaluation of our experiments (Supporting Information), the hybrid may be one of the most promising alternatives to Pt/C catalysts for ORR, HER, and OER in fuel cells and water splitting so far.

3. Conclusion

In summary, we have successfully fabricated a novel N/Co-doped PCP//NRGO hybrid as an advanced electrocatalyst for ORR, HER, and OER by direct pyrolysis of GO-based ZIF-67 framework. The hybrid catalyst exhibits excellent triple electrocatalytic activities for ORR, HER, and OER with good stability in both acidic and basic media, thanks to the excellent porous carbon structure, N/Co-doping effect, introduction of NRGO, and good contact between N/Co-doped PCP and NRGO sheets. Our findings may open up a new avenue for rational design and fabrication of a series of NRGO-based N-doped porous carbon materials incorporating nonprecious metal as multifunctional electrocatalysts for energy conversion and storage applications.

4. Experimental Section

Synthesis of N/Co-doped PCP//NRGO: ZIF-67 samples were prepared according to a previous report.[17] Next, the graphene oxide (GO) was synthesized through chemical exfoliation of graphite powders using a modified Hummers' method.[58] The N/Co-doped PCP//NRGO was prepared by using a simple pyrolysis method with ZIF-67 and GO as precursors. In a typical synthesis of N/Co-doped PCP//NRGO, 20 mg of GO was first dissolved in 40 mL of water by ultrasonic treatment for 1 h to obtain a suspension (0.5 mg mL^{-1}). Next, 0.8 g ZIF-67 was added into the suspension under stirring with heating at 80 °C until completely dry. The obtained GO/ZIF-67 product was then transferred to a furnace and pyrolyzed under Ar atmosphere for 3 h at 900 °C with a rate of 2 °C min^{-1}. The resulting product was dispersed in 2 M H_2SO_4 solution and stirred for 24 h to partially remove metallic cobalt in order to obtain N/Co-doped PCP//NRGO.

Materials Characterization: Characterizations were carried out using field emission scanning electron microscope (FESEM, Hitachi S-4800) equipped with an energy-dispersive X-ray spectroscopy analyzer, transmission electron microscopy (TEM, Hitachi H 9000 NAR), Powder X-ray diffraction (XRD, Scintag XDS 2000), Raman spectroscopy (Renishaw 1000B, Raman Spectroscopy System, 633 nm laser, 1 cm^{-1} spectral resolution.), Infrared (IR, Bruker Vector) spectra, X-ray photoelectron spectroscopy (HP 5950A with Mg Kα), Thermogravimetric analysis (TGA, TA SDT 2960 thermoanalyzer), and Nitrogen adsorption-desorption isotherm measurements (ASAP 2020).

Electrochemical Test: (1) ORR, electrochemical measurements were performed in a standard three-electrode glass cell on a CH Instruments 760D electrochemical workstation using a glassy carbon electrode (GCE) with various catalysts as the working electrode, a Pt wire as counter electrode, and an Ag/AgCl electrode as the reference electrode. 0.1 M KOH was used as electrolyte for rotating ring-disk electrode (RRDE-3A) voltammogram measurements. For the fabrication of the working electrode, 5.0 mg as-synthesized catalyst was mixed with 50 µL Nafion solution (5.0% Nafion in ethanol) and 450 µL deionized water. The mixture was sonicated and 5.0 µL suspension was pipetted out and dropped onto a GCE with a diameter of 3 mm and then fully dried. All electrodes were prepared by depositing the same loading mass of active materials on GCE (diameter: 3 mm) using the same method. Loading amount of the catalysts was 0.714 mg cm^{-2}. Before testing, an Ar/O_2 flow was passed through the electrolyte for at least 30 min to saturate the electrolyte with Ar/O_2. The polarization curves for ORR were performed from 0.1 to − 0.7 V (vs Ag/AgCl) with a scan rate of 5 mV s^{-1} at various rotating speeds from 400 to 2500 rpm. For all of the experiments, the electrodes were cycled at 50 mV s^{-1} until reproducible cyclic voltammograms (CVs) were obtained. To remove the capacitive current of the working electrode, the background current was measured by running the above electrodes in Ar-purged 0.1 M KOH electrolyte and then subtracted from the ORR polarization curve. Thus, the net current of ORR was obtained for evaluation of the ORR activity. The number of electrons and kinetic currents (J_k) involved in the reaction can be calculated using the Koutecky–Levich equation which is expressed by:[59]

$$1/J = 1/J_L + 1/J_K = 1/B\omega^{1/2} + 1/J_K \quad (1)$$

where J is the measured current density, J_k and J_L are the kinetic-limiting and diffusion-limiting current densities, ω is the angular frequency of the rotation in terms of rad·s^{-1}, and B is the Levich slope given by

$$B = 0.62nFC_0(D_0)^{2/3}\nu^{-1/6} \quad (2)$$

$$J_K = nFkC_0 \quad (3)$$

Here, n is the overall number of transferred electrons during O_2 reduction, F is Faraday constant (96 500 C mol^{-1}), C_0 is the bulk concentration of O_2, D_0 is the diffusion coefficient of O_2 in the electrolyte, ν is the kinematic viscosity of the electrolyte, and k is the

electron-transfer rate constant. The RDE experiment was performed using 0.1 M KOH solution saturated with O_2. The number of electrons transferred (n) and J_k were obtained from the slope and intercept of the Koutecky–Levich plots (J^{-1} vs $\omega^{-1/2}$), respectively, and by using parameters $C_0 = 1.2 \times 10^{-6}$ mol cm^{-3}, $D_0 = 1.9 \times 10^{-5}$ cm s^{-1}, and $\nu = 0.01$ cm^2 s^{-1}. In rotating ring disk electrode (RRDE) tests, the ring potential was set to 0.5 V versus Ag/AgCl to oxidize the hydrogen peroxide produced during oxygen reduction on the disk electrode. The electron-transfer number (n) and the hydrogen peroxide yield (H_2O_2%) were calculated from RRDE data using the following equations:[60]

$$n = 4I_d/(I_d + I_r/N) \quad (4)$$

$$H_2O_2(\%) = 200I_r/(N \times I_d) + I_r \quad (5)$$

where I_d and I_r are the disk current and the ring current, respectively, and N is the current collection efficiency of Pt ring and is determined to be 0.424. The electrochemical impedance spectroscopy (EIS) was carried out in the frequency range of 10^{-2} to 10^5 Hz with an AC voltage amplitude of 5 mV in O_2-saturated 0.1 M KOH solution.

(2) HER, electrochemical measurements were performed in a standard three-electrode glass cell on a CH Instruments 760D electrochemical workstation using a GCE with various catalysts as the working electrode, a Pt wire as the counter electrode, and an Ag/AgCl electrode as the reference electrode. 0.5 M H_2SO_4 (purged with pure Ar) was used as electrolyte. For the fabrication of the working electrode, 2.5 mg as-synthesized catalyst was mixed with 50 µL Nafion solution (5.0% Nafion in ethanol) and 450 µL deionized water. The mixture was sonicated and 5.0 µL suspension was pipetted out and dropped onto a glassy carbon electrode with a diameter of 3 mm and then fully dried. Linear sweep voltammetry was carried out from 0.1 to –1 V (vs Ag/AgCl) at 5 mV s^{-1} for the polarization curves and Tafel plots. The catalyst was cycled 50 times by CV until a stable CV curve was obtained before testing.

(3) OER test, electrochemical measurements were performed in a standard three-electrode glass cell on a CH Instruments 760D electrochemical workstation using a GCE with various catalysts as the working electrode, a Pt wire as the counter electrode, and an Ag/AgCl electrode as the reference electrode. 0.1 M KOH was used as electrolyte. For the fabrication of the working electrode, 2.5 mg as-synthesized catalyst was mixed with 50 µL Nafion solution (5.0% Nafion in ethanol) and 450 µL deionized water. The mixture was sonicated and 5.0 µL suspension was pipetted out and dropped onto a glassy carbon electrode with a diameter of 3 mm and then fully dried. All data were collected under O_2 saturation to ensure the O_2/H_2O equilibrium at 1.23 V versus RHE. Linear sweep voltammetry was carried out from 0.1 to 1.1 V (vs Ag/AgCl) at 5 mV s^{-1} for the polarization curves and Tafel plots. The catalyst was cycled 50 times by CV until a stable CV curve was obtained before testing.

Supporting Information

Supporting Information is available from the Wiley Online Library or from the author.

Acknowledgements

Financial support for this work was provided by the U.S. Department of Energy (DE-EE0003208) and the Research Growth Initiative Program of the University of Wisconsin-Milwaukee (UWM).

Received: October 19, 2014
Published online: December 22, 2014

[1] S. Chu, A. Majumdar, *Nature* **2012**, *488*, 294.
[2] a) G. Wu, P. Zelenay, *Acc. Chem. Res.* **2013**, *46*, 1878; b) S. Xie, S. I. Choi, N. Lu, L. T. Roling, J. A. Herron, L. Zhang, J. Park, J. Wang, M. J. Kim, Z. Xie, M. Mavrikakis, Y. Xia, *Nano Lett.* **2014**, *14*, 3570; c) K. A. Kuttiyiel, K. Sasaki, Y. Choi, D. Su, P. Liu, R. R. Adzic, *Nano Lett.* **2012**, *12*, 6266; d) H. Yin, C. Zhang, F. Liu, Y. Hou, *Adv. Funct. Mater.* **2014**, *24*, 2930; e) D. Higgins, M. A. Hoque, M. H. Seo, R. Wang, F. Hassan, J. Y. Choi, M. Pritzker, A. Yu, J. Zhang, Z. Chen, *Adv. Funct. Mater.* **2014**, *24*, 4325.
[3] a) D. J. Li, U. N. Maiti, J. Lim, D. S. Choi, W. J. Lee, Y. Oh, G. Y. Lee, S. O. Kim, *Nano Lett.* **2014**, *14*, 1228; b) H. Wang, H. Dai, *Chem. Soc. Rev.* **2013**, *42*, 3088; c) Z. Chen, D. Cummins, B. N. Reinecke, E. Clark, M. K. Sunkara, T. F. Jaramillo, *Nano Lett.* **2011**, *11*, 4168; d) D. Kong, H. Wang, Z. Lu, Y. Cui, *J. Am. Chem. Soc.* **2014**, *136*, 4897; e) Z. Zhao, H. Wu, H. He, X. Xu, Y. Jin, *Adv. Funct. Mater.* **2014**, *24*, 4698.
[4] a) M. G. Walter, E. L. Warren, J. R. McKone, S. W. Boettcher, Q. Mi, E. A. Santori, N. S. Lewis, *Chem. Rev.* **2010**, *110*, 6446; b) L. Gan, M. Heggen, S. Rudi, P. Strasser, *Nano Lett.* **2012**, *12*, 5423.
[5] a) J. Duan, S. Chen, S. Dai, S. Z. Qiao, *Adv. Funct. Mater.* **2014**, *24*, 2072; b) L. Liao, J. Zhu, X. Bian, L. Zhu, M. D. Scanlon, H. H. Girault, B. Liu, *Adv. Funct. Mater.* **2013**, *23*, 5326.
[6] G. Wu, K. L. More, C. M. Johnston, P. Zelenay, *Science* **2011**, *332*, 443.
[7] D. W. Wang, D. Su, *Energy Environ. Sci.* **2014**, *7*, 576.
[8] a) Y. Li, W. Zhou, H. Wang, L. Xie, Y. Liang, F. Wei, J. C. Idrobo, S. J. Pennycook, H. Dai, *Nat. Nanotechnol.* **2012**, *7*, 394; b) N. Kim, K. S. Kim, N. Jung, L. Brus, P. Kim, *Nano Lett.* **2011**, *11*, 860.
[9] C. Shan, W. Zhao, X. L. Lu, D. J. O'Brien, Y. Li, Z. Cao, A. L. Elias, R. Cruz-Silva, M. Terrones, B. Wei, J. Suhr, *Nano Lett.* **2013**, *13*, 5514.
[10] W. Yang, T. P. Fellinger, M. Antonietti, *J. Am. Chem. Soc.* **2010**, *133*, 206.
[11] K. Gong, F. Du, Z. Xia, M. Durstock, L. Dai, *Science* **2009**, *323*, 760.
[12] H. Wang, Z. Lu, D. Kong, J. Sun, T. M. Hymel, Y. Cui, *ACS Nano* **2014**, *8*, 4940.
[13] Y. Zhao, R. Nakamura, K. Kamiya, S. Nakanishi, K. Hashimoto, *Nat. Commun.* **2013**, *4*, 2390.
[14] M. Jahan, Z. Liu, K. P. Loh, *Adv. Funct. Mater.* **2013**, *23*, 5363.
[15] X. Wang, Q. Weng, X. Liu, X. Wang, D. M. Tang, W. Tian, C. Zhang, W. Yi, D. Liu, Y. Bando, D. Golberg, *Nano Lett.* **2014**, *14*, 1164.
[16] R. Wu, X. Qian, X. Rui, H. Liu, B. Yadian, K. Zhou, J. Wei, Q. Yan, X. Q. Feng, Y. Long, L. Wang, Y. Huang, *Small* **2014**, *10*, 1932.
[17] Z. Jiang, Z. Li, Z. Qin, H. Sun, X. Jiao, D. Chen, *Nanoscale* **2013**, *5*, 11770.
[18] Z. S. Wu, L. Chen, J. Liu, K. Parvez, H. Liang, J. Shu, H. Sachdev, R. Graf, X. Feng, K. Müllen, *Adv. Mater.* **2014**, *26*, 1450.
[19] a) S. Ma, G. A. Goenaga, A. V. Call, D. J. Liu, *Chem. Eur. J.* **2011**, *17*, 2063; b) X. Zou, X. Huang, A. Goswami, R. Silva, B. R. Sathe, E. Mikmeková, T. Asefa, *Angew. Chem.* **2014**, *126*, 4461.
[20] L. Zhi, Y. S. Hu, B. E. Hamaoui, X. Wang, I. Lieberwirth, U. Kolb, J. Maier, K. Müllen, *Adv. Mater.* **2008**, *20*, 1727.
[21] a) M. Sevilla, C. Salinas Martinez-de Lecea, T. Valdes-Solis, E. Morallon, A. B. Fuertes, *Phys. Chem. Chem. Phys.* **2008**, *10*, 1433; b) Q. Gao, C. Zhang, S. Wang, W. Shen, Y. Zhang, H. Xu, Y. Tang, *Chem. Commun.* **2010**, *46*, 6494.
[22] K. Ai, Y. Liu, C. Ruan, L. Lu, G. Lu, *Adv. Mater.* **2013**, *25*, 998.
[23] Y. Chang, F. Hong, C. He, Q. Zhang, J. Liu, *Adv. Mater.* **2013**, *25*, 4794.
[24] Y. Hou, F. Zuo, A. Dagg, P. Feng, *Nano Lett.* **2012**, *12*, 6464.
[25] C. Zhang, N. Mahmood, H. Yin, F. Liu, Y. Hou, *Adv. Mater.* **2013**, *25*, 4932.
[26] P. Chen, T. Y. Xiao, Y. H. Qian, S. S. Li, S. H. Yu, *Adv. Mater.* **2013**, *25*, 3192.

[27] a) H. Sun, X. You, J. Deng, X. Chen, Z. Yang, J. Ren, H. Peng, *Adv. Mater.* **2014**, *26*, 2868; b) M. A. Pimenta, G. Dresselhaus, M. S. Dresselhaus, L. G. Cancado, A. Jorio, R. Saito, *Phys. Chem. Chem. Phys.* **2007**, *9*, 1276.
[28] Z. Lin, G. Waller, Y. Liu, M. Liu, C. P. Wong, *Adv. Energy Mater.* **2012**, *2*, 884.
[29] S. Chen, J. Duan, J. Ran, M. Jaroniec, S. Z. Qiao, *Energy Environ. Sci.* **2013**, *6*, 3693.
[30] a) M. Dominguez, E. Taboada, H. Idriss, E. Molins, J. Llorca, *J. Mater. Chem.* **2010**, *20*, 4875; b) Q. He, Q. Li, S. Khene, X. Ren, F. E. López-Suárez, D. Lozano-Castelló, A. Bueno-López, G. Wu, *J. Phys. Chem. C* **2013**, *117*, 8697.
[31] Y. Hou, F. Zuo, Q. Ma, C. Wang, L. Bartels, P. Feng, *J. Phys. Chem. C* **2012**, *116*, 20132.
[32] Y. Hou, Z. Wen, S. Cui, X. Guo, J. Chen, *Adv. Mater.* **2013**, *25*, 6291.
[33] R. Zheng, Z. Mo, S. Liao, H. Song, Z. Fu, P. Huang, *Carbon* **2014**, *69*, 132.
[34] Q. Li, R. Cao, J. Cho, G. Wu, *Adv. Energy Mater.* **2014**, *4*, 1301415.
[35] G. Nam, J. Park, S. T. Kim, D. B. Shin, N. Park, Y. Kim, J. S. Lee, J. Cho, *Nano Lett.* **2014**, *14*, 1870.
[36] a) L. Lai, J. R. Potts, D. Zhan, L. Wang, C. K. Poh, C. Tang, H. Gong, Z. Shen, J. Lin, R. S. Ruoff, *Energy Environ. Sci.* **2012**, *5*, 7936; b) Y. Zheng, Y. Jiao, Y. Zhu, L. H. Li, Y. Han, Y. Chen, A. Du, M. Jaroniec, S. Z. Qiao, *Nat. Commun.* **2014**, *5*, 3783; c) S. Chen, J. Duan, M. Jaroniec, S. Z. Qiao, *Adv. Mater.* **2014**, *26*, 2925.
[37] Y. Liang, Y. Li, H. Wang, H. Dai, *J. Am. Chem. Soc.* **2013**, *135*, 2013.
[38] X. Chen, F. Li, N. Zhang, L. An, D. Xia, *Phys. Chem. Chem. Phys.* **2013**, *15*, 19330.
[39] H. W. Liang, W. Wei, Z. S. Wu, X. Feng, K. Müllen, *J. Am. Chem. Soc.* **2013**, *135*, 16002.
[40] J. M. Ziegelbauer, T. S. Olson, S. Pylypenko, F. Alamgir, C. Jaye, P. Atanassov, S. Mukerjee, *J. Phys. Chem. C* **2008**, *112*, 8839.
[41] J. Chang, A. J. Bard, *J. Am. Chem. Soc.* **2013**, *136*, 311.
[42] J. Zhang, P. Chen, B. Yuan, W. Ji, Z. Cheng, X. Qiu, *Science* **2013**, *342*, 611.
[43] R. Liu, D. Wu, X. Feng, K. Müllen, *Angew. Chem. Int. Ed.* **2010**, *49*, 2565.
[44] S. Kattel, P. Atanassov, B. Kiefer, *Phys. Chem. Chem. Phys.* **2013**, *15*, 148.
[45] Y. Zhao, K. Kamiya, K. Hashimoto, S. Nakanishi, *Angew. Chem.* **2013**, *125*, 13883.
[46] B. Cao, G. M. Veith, J. C. Neuefeind, R. R. Adzic, P. G. Khalifah, *J. Am. Chem. Soc.* **2013**, *135*, 19186.
[47] J. Deng, P. Ren, D. Deng, L. Yu, F. Yang, X. Bao, *Energy Environ. Sci.* **2014**, *7*, 1919.
[48] Y. Zheng, Y. Jiao, L. H. Li, T. Xing, Y. Chen, M. Jaroniec, S. Z. Qiao, *ACS Nano* **2014**, *8*, 5290.
[49] B. R. Sathe, X. Zou, T. Asefa, *Catal. Sci. Technol.* **2014**, *4*, 2023.
[50] J. Xie, H. Zhang, S. Li, R. Wang, X. Sun, M. Zhou, J. Zhou, X. W. Lou, Y. Xie, *Adv. Mater.* **2013**, *25*, 5807.
[51] S. Mao, Z. Wen, T. Huang, Y. Hou, J. Chen, *Energy Environ. Sci.* **2014**, *7*, 609.
[52] a) M. Li, L. Zhang, Q. Xu, J. Niu, Z. Xia, *J. Catal.* **2014**, *314*, 66; b) J. Masa, W. Xia, I. Sinev, A. Zhao, Z. Sun, S. Grützke, P. Weide, M. Muhler, W. Schuhmann, *Angew. Chem. Int. Ed.* **2014**, *53*, 8508.
[53] G. L. Tian, M. Q. Zhao, D. Yu, X. Y. Kong, J. Q. Huang, Q. Zhang, F. Wei, *Small* **2014**, *10*, 2251.
[54] M. R. Gao, Y. F. Xu, J. Jiang, Y. R. Zheng, S. H. Yu, *J. Am. Chem. Soc.* **2012**, *134*, 2930.
[55] Y. Gorlin, T. F. Jaramillo, *J. Am. Chem. Soc.* **2010**, *132*, 13612.
[56] Y. Lee, J. Suntivich, K. J. May, E. E. Perry, Y. Shao-Horn, *J. Phys. Chem. Lett.* **2012**, *3*, 399.
[57] H. Vrubel, X. Hu, *Angew. Chem. Int. Ed.* **2012**, *51*, 12703.
[58] W. S. Hummers, R. E. Offeman, *J. Am. Chem. Soc.* **1958**, *80*, 1339.
[59] Y. Liang, Y. Li, H. Wang, J. Zhou, J. Wang, T. Regier, H. Dai, *Nat. Mater.* **2011**, *10*, 780.
[60] J. I. Jung, H. Y. Jeong, J. S. Lee, M. G. Kim, J. Cho, *Angew. Chem. Int. Ed.* **2014**, *53*, 4582.